

A Proposal
for
TWO SEPTUM MAGNETS FOR
FORWARD ANGLE PHYSICS
IN HALL A AT TJNAF

Submitted to
The TJNAF Technical Advisory Committee

by the
Hall A
Hypernuclear Collaboration

13 September 1996

Version 1.3

Contents

1	Introduction	1
1.1	Physics Motivations	1
1.2	Performance Requirements	1
1.3	Design Criteria	1
2	Optics Design	3
2.1	General Remarks	3
2.2	General Optic characteristics	3
2.3	Expected Performances	4
3	Magnet Design	5
3.1	Overview	5
3.2	General Description	6
3.2.1	Kinematical Layout	6
3.2.2	General Composition of the Septum Unit	6
3.3	Field Optimization	7
3.4	The Yoke	8
3.5	The Coils	8
3.6	The Cryostat	9
3.6.1	General mechanics	9
3.6.2	Main Current Leads	9
3.6.3	Pumping System	9
3.7	Cryogenic Supply & Cooling System	9
3.7.1	Liquid Helium Circuit	10
3.7.2	Liquid Nitrogen Circuit	10
3.7.3	Cooldown Procedure	10
3.8	Power Supply	10
3.9	Monitoring & Control	11
3.9.1	Magnetic Field Monitoring	11
3.9.2	Temperature Measurements	11
3.9.3	Power Supply Control	11
3.9.4	Vacuum Measurements	11
3.9.5	Cryogenic Supply Parameters	11
3.10	Safety	12
3.10.1	General Aspects	12
3.10.2	Quench Detection	12
3.10.3	Helium Leakeges & Pressure Increase	12
3.10.4	Energy Dissipation	12
3.10.5	Radiation Hardness of the Magnet	12
4	System Integration	13
4.1	Beamline Modifications	13
4.2	Scattering Chamber	13
4.3	Corrector magnet	13
4.4	Sieve Slits	13
4.5	Spectrometer Exit Windows	14
4.6	Support Structure	14

5	Schedule	14
5.1	Manpower	14
5.2	Timetable	15
6	Conclusions	16
7	APPENDIX A - Choice of the Layout	17
8	APPENDIX B - Optics	19
9	APPENDIX C - Issues raised by PAC and Expint	21
9.1	Missing Mass Resolution	21
9.2	Target	21
9.3	Particle Identification	21
9.4	Backgrounds	22
9.5	Septum Magnets heating due to beam radiation	22
9.6	Radiation Hardness	23
9.7	Magnet Activation	23
10	REFERENCES	24

1 Introduction

1.1 Physics Motivations

This design report describes the plan to add two septum magnets to the Hall A HRS spectrometers (one per spectrometer). The addition of the septum magnets allows measurements at very forward angles. Because the Mott cross section peaks at forward angles, there are obvious advantages to going to the MOST forward angle. One such experimental program which utilizes the enhanced virtual photon flux is hypernuclear electroproduction. Because of the small cross sections, the hypernuclear program needs to reach the most favorable kinematics (i.e., the most forward angle) possible.

The main scope of this report is to show the feasibility of adding the septum magnets to the HRS of the Hall A without major modifications of the characteristics of the spectrometers. [Namely the solid angle and the energy resolution should remain approximately unchanged.] Our reference experiment for this will be Proposal 94-107 “High Resolution 1p shell Hypernuclear Spectroscopy” (S. Frullani, F. Garibaldi, P. Markowitz, T. Saito spokespersons) (1) which was conditionally approved by the PAC-9. The condition was to show the feasibility of the use of the septum magnets without a (significant) loss of energy resolution. We will continue to make reference to the Hypernuclear experiment because attaining high resolution at forward angles is crucial for such a program, but it is important to keep in mind that such a general device is useful for a variety of other experiments. It will enhance greatly the experimental program for Hall A, especially for programs such as the parity violating scattering and the virtual compton scattering (4).

1.2 Performance Requirements

Septum magnets are needed for the HRS2 Spectrometers in Hall A to allow experiments using scattering angles smaller than the minimum angle of 12.5° . In fact the cross sections for the hypernuclear experiment go down sharply with the increasing scattering angle so, to enhance the virtual photon flux, going to the most forward scattering angle is very important (6° is sufficient). To first produce and second keep a reasonable kaon survival fraction, the particles momenta have to be fairly high ($\sim 1.8\text{GeV}/c$ for the electrons and $\sim 2\text{GeV}/c$ for the kaons). The angular acceptance should be ~ 4.5 mrad to keep the solid angle of the spectrometer reasonable. Good resolution in missing mass is needed, so the momentum resolution should be as small as possible ($< 2. \times 10^{-4}$) Moreover, the aim is to have a general purpose device, so particles scattered at the new minimum angle should also reach momenta as high as the maximum central momentum analyzable by the HRS2 (4 GeV/c). The angular range of use for the septum magnets should also cover the full range from 6° to 12.5° , the “normal” HRS setup minimum angle (again, for all momenta upto 4 GeV/c).

1.3 Design Criteria

Physically, the first quadrupole ($Q1$) of the spectrometers cannot be moved closer than 12.5° to the beam without hitting the beam pipe.(3) The idea is to move the target upstream a suitable distance and to insert a horizontal-bending septum magnet before the point element in the spectrometers in such a way that the target

seems to be situated on the optical axis of the two spectrometers (Fig.1). This is precisely true only for the central momentum of the spectrometer, for other momenta the target will appear to be shifted sideways.

The septum has to be designed in such a way that the trajectory of the particle in Fig. 2, scattered at the acceptance central angle ϕ would overlap, after being bent, the line originating from O (old target position) and making an angle θ ($\geq 12.5^\circ$) with the beam line. In addition the septum gap has to be designed to accept all particles scattered in the acceptance cone (see Fig.2 for the case $\phi = 6^\circ$; $\theta = 12.5^\circ$ and acceptance in the midplane plane = 24 mrad).

It has been shown therefore (see Appendix A) that the septum design is almost completely determined by two parameters: the distance d between the old and new position of the target (80 cm) and the magnet thickness T (the distance between the septum gap and the beam pipe) (Fig. 2). A choice of d = 80 cm and T = 2.5 cm was made. Using these values we can get a geometrical acceptance of 4.5 msr. Moreover, with a reasonable field integral, particles of momentum up to 4 GeV/c can be analyzed for angles from 6° to 12.5° .

The mechanical design of the septum is determined more by the Hall A geometrical layout and the maximum current density available in superconducting coils than by optic considerations. The septum, because of the short length and small bend angle, can be treated as a perturbation to the optical properties of HRS. On the other hand, the limited room available, the required geometrical acceptance and the difficulty of obtaining highly homogenous magnetic fields with thin coils set severe constraints on the septum design.

In Table 1 we summarize the dimensions of the septum:

Table 1 Septum Dimensions

Length *	88. cm
Height of the gap	25. cm
Width of gap entrance edge	10.4 cm
Width of gap exit edge	18.4 cm
Angular acceptance	4.7 msr
Magnetic length	84. cm

(* length includes length of the coils outside the yoke)

In Table 2 we report the septum parameters that depend on momentum and scattering angle of the detected particles. P is the scattered particle momentum, θ is the scattering angle, β is the horizontal bending angle of the septum magnet, the magnetic field (in the region of constant field) and field integral over the path are B_0 and $B \cdot dl$. R is the horizontal radius of curvature for the septum magnet.

Table 2 Septum Parameters

P	θ	β	R	$B \cdot dl$	B_0
GeV/c	degrees	degrees	cm	Tesla-m	Tesla
2	6	6.5	740.8	0.76	0.9
4	12.5	11.9	404.6	1.39	1.65
4	6	6.5	740.8	1.51	1.8
4	12.5	11.9	404.6	2.77	3.3

2 Optics Design

2.1 General Remarks

We evaluated the effect of the addition of the septum to HRS spectrometer. This effect should ideally be a small perturbation of the HRS optic properties. The principle effect is the addition of small non-“midplane symmetric” terms to the transfer matrix. It will be shown below, that the perturbation to the HRS optical properties caused by the presence of the septum is indeed small. This can be predicted by considering that both the new elements introduced, a new drift distance to include the septum and the field of the septum itself, are relatively small in comparison .

2.2 General Optic characteristics

The major changes necessary in the HRS system to add the septum consist of increasing the Q3 quadrupole field and slightly decreasing the Q1 quadrupole field. The first change is needed to compensate for the shift of the focal point for the central momentum caused by the larger first drift distance. The second change is needed to keep the first order resolving power constant and avoid losing particles in the transverse plane. In this way, the HRS first order optical properties are maintained. Above all, the ratio D/m , that determines the resolving power, is still close to 5, and the $\langle y|\phi \rangle$ matrix element is still small. This last property is extremely important because the resolution of the y_0 interaction point coordinate, determined essentially by $\langle y|\phi \rangle$, is enhanced at very forward particle scattering angles by geometric reasons.

Table 3 @ GeV/c Quadrupole Settings

	HRS	HRS + Septum
Q1 field at aperture	0.6882	0.6075
Q2 field at aperture	0.4696	0.5015
Q3 field at aperture	0.4553	0.5770
Target to Q1 drift	167.064	245.942

(including septum length for HRS + Septum case)

Table 3 shows the differences in the quadrupole fields between HRS and HRS + septum spectrometer. Drift distances are in cm and magnetic fields are in Tesla. This table refers to a central momentum of the scattered particles equal to 2 GeV/c. For comparison, the corresponding values of the HRS without septum are also reported. In the same table, the different drift distances from the target to Q1 are also shown. The y_0 acceptance along the perpendicular to the central trajectory is 5 cm, which means that a target length of $5 \times \sin 6^\circ = 50$ cm can be accommodated.

The first order matrix elements, as calculated by TRANSPORT are given below:

$$\begin{pmatrix} -2.81214 & 0.00000 & 0.00000 & 0.00000 & 14.06069 \\ -3.18504 & -0.35560 & 0.00000 & 0.00000 & 24.68781 \\ 0.00000 & 0.00000 & 1.01244 & 0.04074 & 0.12918 \\ 0.00000 & 0.00000 & 12.80820 & 1.50307 & 0.51663 \\ 2.46416 & -0.50000 & 0.11314 & 0.01731 & -0.63948 \\ 0.00000 & 0.00000 & 0.00000 & 0.00000 & 1.00000 \end{pmatrix}_{septum} \begin{pmatrix} x \\ \theta \\ y \\ \phi \\ \delta \end{pmatrix}_{target} = \begin{pmatrix} x \\ \theta \\ y \\ \phi \\ \delta \end{pmatrix}_{focal_plane}$$

Again, the resolution of the y_0 interaction point coordinate is determined essentially by $\langle y|\phi \rangle$. At very forward particle scattering angles, geometric arguments limit the resolution along the incident beam axis. Table 4 shows the value of $\langle y|\phi \rangle$ as a function of δ , the momentum relative to the central momentum (values calculated by the program RAYTRACE):

Table 4 $\langle y|\phi \rangle$ as a function of δ

Momentum (GeV/c)	1.900	1.949	1.988	2.047	2.096
$\langle y \phi \rangle$ (cm/rad)	-2.826	-1.182	0.313	0.308	-3.031

As discussed in Appendix B, for studying the effects of inserting the septum in the spectrometer optics, we have performed standard optical calculations using Raytrace and Snake codes, and taking into account the effects of multiple scattering from the target, the target window and the spectrometer exit window.

2.3 Expected Performances

Standard techniques and modelling (described in detail in Appendix B) shows that the perturbation of the septum to the HRS spectrometer features is small. As a matter of fact the momentum and target coordinate resolutions of the system septum + HRS obtained in this way (considering only fixed momentum particles (see appendix B)) is quite close to the resolutions of the HRS alone (fig.24). The calculations mentioned in the previous paragraph and described in Appendix B, give the following results: the momentum resolution is expected to be 1.2×10^{-4} using kapton for the spectrometer exit window, and 1.35×10^{-4} for the Ti one. [A kapton window is already planned separately to maximize the HRS performance.] The resolution in θ is 0.96 mr and 1.26 mr respectively. The effect of the multiple scattering from the target and the target window (waterfall target) is very small. In fact resolution in θ remains 0.96 mrad if we take into account the multiple scattering from the target. The influence of the target window is of the same order. The resolution in y is equal to 0.365 mm for the kapton window and 0.435 mm for the Ti one. The resolution in ϕ is respectively, 0.38 mr and 0.50 mr. In Tab. 5 we summarize the expected performances of the new HRS + septum spectrometer as compared to the HRS ones.

Table 5 Expected Performances

	HRS	HRS(a)	Septum	Septum(r)
Angular acceptance	7.3 msrd	5.5 msrd	4.5	3.4
Momentum resolution	1.0×10^{-4}	2.0×10^{-4}	1.2×10^{-4}	2.0×10^{-4}
Minimum scattering angle	12.5°	12.5°	6°	6°
Momentum Range	0.4-4 GeV/c	0.4-4 GeV/c	0.4-4 GeV/c	0.4-4 GeV/c

‘HRS’ and ‘septum’ means the design parameters in the CDR (plus the addition of the septum) while HRS(a) is the HRS presently achieved performances and septum(r), consequent implied realistic performances.

We have performed a Monte Carlo calculation to evaluate the missing mass resolution for the hypernuclear experiment. The result is (FWHM) ~ 630 KeV (for a 4σ beam resolution of $E_{beam} = 1 \times 10^{-4}$, a momentum resolution of 2.0×10^{-4} , and an angular error of 1 mr (Fig. 3). This value is sufficient for our experiment. In fact the best energy resolution attained until now, by means of hadron probes, is in the range 1.6 - 2 MeV. So this represents a big improvement in energy resolution. Improvements in energy resolution in the past resulted in a better understanding of the hypernuclear structure and of the Λ -N interaction(17). Moreover the use, for the first time, of the electromagnetic probe, allowing the excitation of new states and the production of hypernuclei not available otherwise, is expected to reveal new aspects of hypernuclear structure(1).

3 Magnet Design

3.1 Overview

The main design parameters for the spectrometer magnets are given in Tables 1, 2, and 3. Taking into account the limited space available for the septum (about 1.5 m along the beam axis), the required aperture width, and the desired product $B \cdot l = 2.4$ T-m, a magnet with warm coils would saturate before satisfying the conditions.

To optimize the design of the superconducting magnet, two additional limiting factors were taken into account:

- i) minimization of fringing fields in the beam pipe;
- ii) possibility of independent choice of momenta and angles for the two arms.

To minimize fringing fields the main dipole field of the magnet must be screened. There are two possible ways to screen stationary magnetic fields:

- by nonsaturated iron (passive screening);
- by another coil of appropriate geometry and current distribution (active screening).

The iron-less option of SC- dipoles with active screening has been considered in several papers and the attractiveness of such a SC-magnet was demonstrated, but for this case the applicability of this option looks problematic.

The best design for the septum magnets is an iron-core with SC-coils. The first "window-frame type" iron core dipole with superconducting coils was constructed by G.Danby at BNL in 1971 (7). This magnet generated a dipole field of 4.2 Tesla in an aperture of about 5 cm . Integral field inhomogeneity of about 0.01% was provided at the level of 3.7 T after using additional correcting coils.

Iron-shaped field magnets of different types have been investigated at the Laboratory of High Energies of the Joint Institute for Nuclear Research in Dubna since 1974 . The first relativistic heavy ion superferric synchrotron — the Nuclotron was designed and constructed at the LHE during 1987-92 using this technology. The experience from operating the Nuclotron has shown a high reliability and efficiency for its superconducting magnetic systems, which include about 200 SC-magnets as well as twelve 6 kA helium-cooled main current leads, 234 100-Amp current leads for correcting coils, many other special superconducting devices and elements for power supply, quench detection, stored energy deposition etc. All equipment is controlled by the computer system.

Typically a SC-magnet with an iron-shaped field consists of a cold iron yoke, superconducting coils (different types of superconducting cable and cooling are used), liquid nitrogen system, heat superinsulation and a vacuum tank. Current leads, liquid He and liquid nitrogen headers as well as equipment for temperature and vacuum measurements, magnetic field monitoring, quench detection are also the main components of any SC-magnet. To satisfy the conditions specified for the two-arm forward spectrometer two options of iron-shaped field SC-septum were considered:

1. installation of both dipoles inside a common cryostat;
2. two completely independent magnets.

The first option provides a more compact installation of the magnets and may cover smaller forward angles, but the axial position of the magnets is essentially fixed. Angular position of the septa can be changed but mechanical equipment of the cryostat is more complicated as well as requiring the sizes of the cryostat to be bigger.

Finally therefore, the option of two independent iron-shaped field SC dipoles was chosen as basic concept for the design.

3.2 General Description

3.2.1 Kinematical Layout

General layouts of the septum kinematics and the basic sizes of the iron yoke are shown in Figs. 4,5. Asymmetrical iron yokes with an additional half-ring hole along the beam pipe are used to provide the analysis of the secondary particles at an angle of 6° . Taking into account the “useful” area of the aperture needed for the scattered particles, a varying horizontal aperture of the magnets is suggested. Such a decision also gives an additional degree of freedom for varying the iron yoke parameters used for the magnetic field optimization.

3.2.2 General Composition of the Septum Unit

The general view of the septum magnet unit inside the cryostat is shown in Fig. 6. The iron yoke is supported by a single column placed at the center-of-mass of the yoke. Two helium cooled current leads are mounted at the top of the cryostat. The vertical size between the upper ends of the current leads and the septum axis is 106 cm. The total vertical size of the unit is 180.5 cm. Total axial size of the cryostat is 95.0 cm. The axial length of the yoke is 73 cm. The vacuum vessel and two intermediate temperature screens have the diameters of 86 cm, 80 cm, 75 cm respectively in the regular part (opposite to the beam pipe). The side oriented toward the beam pipe is made as a plane surface with an axial hole with a half-ring cross-section.

The cross-section of the yoke is a closed “C-type”. The wall on the beam pipe side has a linearly varying thickness. Due to this fact the ends of SC-winding at the front and rear part of the magnet are different. The front end of the coils is “saddleshaped” and the opposite one is “plane-type”. The coils are made of a “rutherford type” superconducting cable.

3.3 Field Optimization

Preliminary calculations of the magnetic field distribution were made using the MAGSYS-2d computer code. After that more precise calculations were carried out using TOSCA. In optimizing the window sizes, the yoke and the coil end shape geometry the following design considerations were used:

- minimal deviations of the computed field distribution from the designed one over the entire dynamical range of the fields,
- stability of the integral effective magnetic length,
- efficient magnetic circuit for the yoke to minimize iron volume and weight,
- magnetostatic forces on the coils, septum wall and support system
- fringing fields in the region of the unscattered beam.

Before showing the result it is important to note that the trajectories of the particles are not symmetric with respect to the center of the septum. As a matter of fact, the central trajectory crosses (at the entrance) the region of the septum closest to the beam pipe, then (after passing the center of the septum) crosses the opposite region (Fig. 4). It is therefore better to focus on the behavior of the magnetic field in the regions crossed by particles. It could be dangerous to study some parameters (the homogeneity for example), with respect to the value assumed at the center of the magnet. For brevity, the fields generated by only two current density values will be shown in detail here:

- a) current density equal to 14.6 KA/cm^2 corresponding to a magnetic field integral value of 1.58 Teslameters (particle momentum equal to 4 Gev/c; scattering angle 6°).
- b) Current density equal to 28 KA/cm^2 corresponding to a magnetic field integral value of 2.89 Teslameter (particle momentum equal to 4 Gev/c; scattering angle 12.5°). The case a) is representative of cases in which no saturation is reached inside the iron. Case b), on the other hand, is the maximum magnetic field the septum is supposed to generate. The coordinate system used in the graphs for this section has its origin at the center point of the septum (Fig.7). The z-axis lays in the center of the septum and is directed from the origin to the entrance face of the magnet. The entrance face of the septum has the coordinate $z = -36$; the exit one coordinate is $z = 36$. The x-axis lays on the septum midplane and is directed from the center to the beam pipe. The x coordinate of the coil near the beam pipe is $x = 9.2$, the x coordinate of the opposite coil decreases linearly from $x = -1.2$ (at the septum entrance) to $x = -9.2$ (at the septum exit). The y-axis is perpendicular to the midplane.

Fig. 8 shows the magnetic field behaviour along the longitudinal (z) coordinate of the septum in the midplane ($y=0$) and at the center of the septum ($x=0$). Fig. 9, Fig. 10 and Fig. 11 show (for 6°) the trend of the magnetic field along the transverse coordinate ($z=\text{constant}$) at the center of the septum, at the exit surface and at the intermediate position between these two. Fig. 12 and Fig. 13 are the analogs of Fig. 8 and 9 for the case at 12.5° . Apart from Fig. 8 and 12, the central abscissa of all the graphs coincides with the intersection of the central trajectory with the plane $z=\text{const}$.

The inhomogeneity of the field in the case at 12.5° appears at first glance too high but is still below the desired value (less than 1 per cent). That is shown in Fig. 14 that plots the maximum field inhomogeneity detected in the region crossed by

particles as a function of the longitudinal coordinate of the septum. The differences between the 6 degree and 12.5 degree case are of course due to the much higher iron saturation that occur in 12.5. As a matter of fact the maximum value of the modulo of the magnetic induction is 5.9 Tesla in case 12.5 and 4.4 in case 6.

In both cases the higher saturation is reached at the exit surface of the septum ($z=36$), because the peculiar shape of the coils makes them close to the pole. However in both cases the saturated iron region does not stretch very much: as an example Fig. 15 shows the value of the magnetic induction at the center of the septum both in the gap and in the iron ($-5.2 < x < 9.2$). Note that the saturation is higher in the iron closer to the beampipe because its thickness is smaller.

Fig 16 shows the stray field generated on the beam pipe in case 6 degrees. It is the maximum field that can be generated on the beam line because, in the large scattering angle ($\theta = 12.5^\circ$) case, the septum is far from the beam pipe. Fig. 17 shows the value of the magnetic field integral as a function of the current density. As can be easily checked for cases a) and b) above (see also Table 2), the magnetic length of the septum (defined as the distance L_m that makes the product $B_0 \cdot L_m$ equal to the magnetic field integral inside the septum) is kept constant along the dynamic range of the fields (B_0 is the field in the constant region). To minimize the stray field in the beam pipe we will put corrector coil(s) (see par. 4.3)

3.4 The Yoke

The yoke (for each septum) is fabricated of a low-carbon steel. It could be nonlaminated because a quasi-stationary mode of operation is used. The material for the yoke is certified by industrial standards. The basic sizes of the yoke are shown in Fig. 6. The yoke consists of two parts which are symmetrical with respect to the horizontal plane. Total weight of the yoke is about 1700 kg. The tolerances on the dimensions follow from the magnetic field calculations and are provided by precise machining. The window is manufactured with a size accuracy of 0.02 mm, and the iron is similarly manufactured with the total axial length having an accuracy of 0.5 mm.

3.5 The Coils

The SC-coils are made of a superconducting cable usually known as “Rutherford type”. The cable consists of SC strands (usually an 50/50 alloy of NbTi) and stabilizing copper wires. The cable for the SC-coils has a rectangular cross-section with dimensions of $0.96 \times 5.69 \text{ mm}^2$ made of 13 SC strands and 10 copper stabilizing wires, 0.5 mm in diameter. The ratio of superconductor-to-copper in each strand is 1:1.5. Each wire is covered by a tin-lead alloy. The profile of the cross-section is formed by a special cable making machine. The cable is insulated by a kapton film 0.08 mm thick and a glass tape 0.1 mm thick. The glass tape is impregnated by a special glue (VT-12) that is polymerized at 125° C .

The technology of SC cable and SC coil production for the septa is similar to that used under large scale production of dipole magnets for the SC synchrotrons at the LHE JINR. Average current densities of 350 A/mm^2 were routinely provided with this design. The SC coils are wound in two layers and cooled indirectly. The ends of the coils have a different shape. The “saddletype” shape of the winding is used at the entrance plane of the magnet. In this case the total cross sectional size of the winding at the edge of magnet is equal to the size of the window in the yoke, but an

additional space of one half of the vertical aperture is needed in the axial direction. The opposite end of the winding is flattened on the yoke to minimize the physical length of the magnet. The endshapes of the coils are shown in Fig.6 respectively.

The coils are operated at 2000 A, or an operating condition approximately 5/8 of the cable critical current. The operating temperature is specified as 4.5 K. The philosophy of the coil design follows a low-risk design concept.

3.6 The Cryostat

3.6.1 General mechanics

The cryostat consists of an external vacuum vessel and two intermediate screens at temperatures of 20 K and liquid nitrogen respectively. The vacuum vessel is fabricated of stainless steel. The intermediate screens are made of copper. All materials are certified by industrial standards. Relative distances between the screens and vacuum vessel are provided by means of special fixing screws. The magnet support column is designed to provide both mechanical rigidity and the minimal heat leak. Total heat leaks due to cold mass supports are estimated as 0.4 W at the temperature of 4.5 K. Mechanical stability of the semi-cylindrical shell of the vacuum vessel with respect to atmospheric pressure was calculated and the shell thickness of 1.7 mm was chosen. This provides a safety factor on collapse of approximately 2 and should be compatible with the CEBAF Vacuum Vessel Standard.

3.6.2 Main Current Leads

Helium cooled current leads of the type similar to what were designed, constructed and used at the Nuclotron are proposed for the septum magnets. The current leads of the Nuclotron can provide a dc mode of current supply with amplitudes up to 9 kA. The maximum value of the current for this septum design is 1.75 kA. The refrigeration power needed for the current leads at the level of 2 kA is about 4.0 W.

3.6.3 Pumping System

The pumping system should provide a pressure of $10^{-5} - 10^{-6}$ inside the vacuum vessel before the coolant is run. The pumping system specification depends on the general vacuum system of the TJNAF Hall A.

3.7 Cryogenic Supply & Cooling System

The cooling system final design should be in agreement with the CEBAF Hall A cryogenic equipment. The heat loads at 4.5 K are as follows: (per each septum in W)

Heat Loads (at 4.5 K)

radiation	0.42
supports	0.40
residual gas	0.05
current leads	4.00
LHe inlet	0.8
other	1.25
<hr/>	
TOTAL	6.9
shield 20 K	0.3
liquid nitrogen shield	55.0

Summary: Refrigeration/liquifaction power of 20 W is sufficient for both magnets cryogenic supply at 4.5 K.

3.7.1 Liquid Helium Circuit

The cooling of the magnet yoke and copper holders is provided by LHe circulation through pipes at a pressure drop of 0.2 – 0.3 bar between inlet and outlet. The pressure of cool helium gas at the beginning of the magnet cooling is 1.5 – 1.7 bar. In the stationary state the LHe flow rate is 20 – 30 g/min per each magnet.

3.7.2 Liquid Nitrogen Circuit

The cooling of the nitrogen screen is provided by LN circulation at a speed 50 g/min approximately through the copper pipes welded to the copper screen. The pressure of the cool nitrogen gas at the beginning of the magnet cooling is 2 bar. The operational pressure drop in stationary mode is 0.4 bar.

3.7.3 Cooldown Procedure

The cooldown procedure has two stages: preliminary and operating. At the first stage all the parts of the magnet are cooled by the gas helium flow. The He gas pressure is 1.5 – 2 bar and is at a temperature of 80 – 90 K in the heatexchanger placed in the LN bath. This stage takes 15 – 20 hours. After the cooling from room temperature level to 110 – 120 K the helium gas in the pipes of the LN screen is replaced by liquid nitrogen and in the pipes of the magnet by LHe flow. The 20 K screen is cooled by a part of the return LHe flow. The relatively low heat loads of the magnets permit one to use a cryo-refrigerator micromachine of the type model CGR 511 or other cryogenic equipment of TJNAF HALL A.

3.8 Power Supply

The electrical power system for any superconducting magnet consists of a power supply, quench detection system, energy dump circuit and a control system. These items have to be treated as a whole at the design stage although they can be produced separately. The necessary voltage of the power supply depends on a desired time for a drive current rise and the coil inductance: $V = L \cdot di/dt$. If we assume a reasonable time of the maximum design magnetic field excitation of 5 minutes, the peak voltage of the power supply (for each magnet) should be not less than $V=0.7$

volts. Substantially higher voltage should be provided for rapid evacuation of stored energy from the magnet in the case of a quench. Stabilization of the supply current at the level of 10^{-3} (10^{-4}) is provided.

3.9 Monitoring & Control

3.9.1 Magnetic Field Monitoring

To provide monitoring of the magnetic field each unit of the septum magnet is equipped with an NMR probe and a connector at the vacuum vessel. This measurement (which could be used as additional test of the septum magnets operational parameters) needs proper electronics and instrumentation. There is an existing NMR probe system in place. Additional probes can be added to the system in a trivial fashion. There are two modes which can be considered:

- on-line monitoring during the data taking run;
- probing the magnetic field only during the test period simultaneously with measurements of the supply current amplitude and after that the last parameter will be the main measurable quantity.

3.9.2 Temperature Measurements

Special carbon resistors developed at the Laboratory of High Energy are used for temperature measurements of the magnets cold parts. The resistors provide temperature measurements with an accuracy of ± 1 K in a range of 300 – 4.5 K. Additional temperature monitoring can be done during cooldown by measurements of the main coil resistance.

3.9.3 Power Supply Control

A programmable electronics is proposed for the power supply control. Moreover the power supply source is equipped with a standard system of current and voltage measurement and handle control. A controlled fast discharge circuit based on a thyristor and dump resistor is used for stored energy dissipation. More detailed specification of the power control system will be done at the stage of final technical and economic design.

3.9.4 Vacuum Measurements

The pressure in the vacuum vessel is measured directly by standard vacuum gauges. The gauges are installed at the vacuum vessel. If the pressure in the vacuum vessel is than higher 10^{-3} tor then the alarm signal to the power supply control system is generated.

3.9.5 Cryogenic Supply Parameters

Monitoring of the cryogenic supply parameters such as pressure, temperature of nitrogen and helium should be included in the main specification list.

3.10 Safety

3.10.1 General Aspects

In all aspects the equipment to be used at TJNAF for the experiments shall meet the relevant TJNAF safety regulations.

3.10.2 Quench Detection

The SC coil of the magnet is divided into two symmetrical parts with respect to the median plane of the magnet. This makes it possible to use these parts for detection of the presence of a normal zone in the superconductor. The voltage of each half of the coil is measured by a bridge circuit and if the difference is larger 50 mV then the alarm signal will be generated and the quench protection system will be activated.

3.10.3 Helium Leakeges & Pressure Increase

There is some significant volume of cryogenic liquid in the septum magnet system. If the liquid helium leaked into the cryostat it would vaporize and the potential would exist to raise the cryostat pressure. The increase of pressure inside the vacuum volume will be regulated by the vacuum monitoring system at an early stage. The electric signal switching the power supply off and the energy dissipating circuit on will be generated if the pressure inside the vacuum vessel exceeds 10^{-3} Torr. To prevent a pressure growth above 1 atm a special membrane is used.

3.10.4 Energy Dissipation

The stored energy is dissipated by an external resistor (70 %) and by a short circuit copper turn around the SC coil. The turn effectively dissipates 20 – 25 % of the stored energy due to currents induced during the fast energy evacuation. In the case of total stored energy dissipation directly in the magnet the temperature of the coils reaches 125° K. This case is also not dangerous for the septum elements.

3.10.5 Radiation Hardness of the Magnet

Radiation hardness of the magnet: Estimates were made for the following beam conditions: beam energy $E=4$ GeV, aperture of the magnet $r=18.4$ cm, efficiency of target (200 mg) $\eta = 0.01$, distance between target and magnet $l = 80$ cm, beam current = 200 μ A (continuous beam). The main conclusions are:

1. about 0.42-0.44 W of cooling power is needed to compensate radiation heat losses.
2. there are no practical limits for the septum magnet operation under above mentioned conditions taking into account radiation hardness of isolating materials to be used for the coils fabrication.

This simulation was also repeated with G.Stapleton at TJNAF, and provided similar results.

4 System Integration

4.1 Beamline Modifications

The addition of the septum magnets involves the cryogenics for the magnets, the magnets and their support, shifting the target chamber upstream by 80 cm, adding new beampipe through the septa, and shifting existing equipment (the dump raster and last beam position monitor) upstream. The design work is underway, although until the final magnet drawings are completed, support structure cannot be built. The timetable calls for the design to be complete in 6 to 12 months.

4.2 Scattering Chamber

The shift in the target position (by -80.0 cm) and the narrow range of scattering angles ($6 < \theta < 12.5$) over which the septum is used with mean that the new scattering chamber does not need to be as complicated as the standard scattering chamber. The targets will require a chamber with a diameter of 60 cm, centered about the new target position.

The target chamber is also under design, and the chamber is expected to be built within the next several months. The design is specifically for use with the septum magnets, and allows for the possibility of use of a cryogenic target as well as the present solid targets and waterfall target. The height of the chamber will be essentially unchanged from the present height of 1.2 meters.

4.3 Corrector magnet

In spite of efforts to minimize them, the stray fields from the septum magnets are sufficient to deflect the beam about 0.4° . This means the downstream beam envelope will hit the wall of the beam pipe. To correct this, we have to deflect the beam back to the center of the beampipe in advance of the beam dump. The integral of the magnetic field along the beam line caused by the septa is estimated from the magnetic field calculation to be $0.1 \text{ T}\cdot\text{m}$. The space for the correction magnet is available most easily between the scattering chamber and the septum magnets. The magnet has to generate the magnetic field along the beam line which can cancel the deflection by the stray field of the septum magnets. It is desirable that the correction magnet in turn generate as small as possible stray fields along the way to the septa. Because these two requirements are contradictory and the available space is very small, we have to devise a magnet for the severe geometrical condition. The detail will strongly depend on the design of the scattering chamber. Figure 4 shows one of the possible positions. The field and the length are 0.5 T and 0.2 m, respectively.

4.4 Sieve Slits

Sieve slits are planned for determining the angular resolution and acceptance of the spectrometer and for studying the “depth of focus” problem. The sieve slits will be a solid piece, for both arms, with a hole in the center for the unscattered beam and hole patterns on both sides for the spectrometers. This simple apparatus will also enable us to check the angular alignment of the two spectrometers relative to each other (centered about the beam).

4.5 Spectrometer Exit Windows

The HRS spectrometers are designed to achieve momentum resolutions of the order of 10^{-4} and angular resolutions of 1–2 mr. These resolutions are necessary to achieve the best missing mass resolution. It is therefore critical that all contributions to the uncertainty of the particle momenta are minimized. One of the largest contributions is multiple scattering of the particles in the vacuum windows of the spectrometer. The distribution of the multiply scattered particles can be represented as a Gaussian with a width given by:

$$\theta_0 = \frac{13.6 MeV}{\beta cp} z \sqrt{x/X_0} [1 + 0.038 \ln(x/X_0)]$$

To achieve the optical quality the spectrometers are capable of, thin vacuum windows are being built capable of withstanding atmospheric pressures. Windows of this type and of a similar size have already been built at the university of Mainz. The technique used mylar windows reinforced with kevlar thread glued directly onto the mylar surface. Starting with the design used at the university of Mainz, the necessary modifications and improvements for windows which can be installed at TJNAF are underway.

The tasks associated with this project require the application of many basic principles which are taught in elementary and advanced physics courses such as mechanics (stress and sheer strain), statistical physics (diffusion) and the interaction of radiation with matter (multiple scattering and energy loss). The construction of these windows involves the development of the necessary tools to manufacture the window material the development of a small test apparatus where prototypes can be tested for strength and tightness and a full scale test stand where the final window in can be tested. The project is estimated to take 1–1.5 years.

4.6 Support Structure

The support structure for the magnets consists of a three-point table, with two legs supported on the HRS spectrometers and one leg using the old target pivot (for the nominal targets). The three point system is easier to level than a four-point system and provides a means of adjusting the height.

Total weight of the magnets (estimated at 1700 kg apiece), the scattering chamber, and related equipment is less than 5 tons. The table (a large flat aluminum plate) has the ability to make small adjustments to the magnet positions via threaded position screws. The timetable for the design is after final drawings of the magnets are finished and fabrication is underway.

5 Schedule

5.1 Manpower

The main universities and groups building and commissioning the septum are INFN/Sanita', INFN/Lecce, INFN/Bari, University of Maryland, Tohoku University, and Florida International University. Together, these institutions have a total of 19 research physicists working on the septum construction and 12 technicians (of course this is not the number of FTEs but the number of active workers). Additionally, the complete list of groups participating in the experiment is given below:

Participating Universities

INFN/Sanita'	Florida International University
INFN/BARI	University of Maryland
INFN/Lecce	Tohoku University
MIT	UVa
Yerevan	U. Georgia
American University	Rutgers
William and Mary	California State U.
U. New Hampshire	Norfolk State U.
Hampton University	Prague Nuc.Phys.Inst.

All told, these institutions have 36 PhD scientists on the experiment proposal.

5.2 Timetable

The total time for building the septa is estimated as 15 – 17 months. The main stages are broken down as:

i) final drawings will take 2 – 3 months. This stage involves preparing the detailed drawings of the septum specification and providing procurement of materials for fabrication of mechanical and electrical parts.

ii) fabrication will require 5 months for the septum elements, including the SC-cable with the design parameters and forming the SC-coils.

iii) assembling and stand tests. The duration of this stage is estimated as 3 – 4 months. It includes fullscale assembly of the septum magnet units on test stands and tests of vacuum, cryogenics, electrical and mechanical systems as well as magnetic measurements. The design parameters of the septum units should be obtained after this work is completed.

iv) transportation of the equipment will require about 1 month

v) installation and commissioning in the Test Lab at TJNAF is estimated as 1 – 2 months.

Timetable

Stage	Time (months)	Tasks
i	2–3	final drawings
ii	5	fabrication
iii	3–4	assembly
iv	1	transportation
v	1–2	installation
TOTAL	12–15 months	

6 Conclusions

The design of the septum magnet satisfies the requirements listed in Table 1. The addition of the septum magnets will enable the HRS spectrometers in Hall A to perform measurements at scattering angles smaller than 12.5° , in particular angles as small as 6° while preserving the possibility of varying the angle up to 12.5° for particle momenta up to 4 GeV/c.

The magnets are an addition to the Hall A infrastructure which are useful for a range of experiments; the optics of the HRS spectrometers are preserved. Apart from a small reduction of the solid angle ($\sim 30\%$) the performance of the spectrometers is essentially unchanged.

The proposed magnet construction schedule fits the Jefferson Lab calendar in that the septum magnets will be ready to be installed shortly after Hall A has achieved full capability (Day 1, in the language of the Hall A EXPINT committee). The manpower of the collaboration is adequate for the scope of the project, and the collaboration has identified the required external resources.

7 APPENDIX A - Choice of the Layout

The septum shape is almost completely determined by two parameters: the distance \mathbf{d} between the old and the new position of the target, (80 cm in Fig.2), and the magnet thickness \mathbf{T} between the septum gap and the beam pipe, (2.5 cm. in Fig. 2). \mathbf{d} determines:

- 1 The angular acceptance, that is equal to the HRS original design scaled by the factor $D/135$ (D is the length in cm of the trajectory between the new target and $Q1$, 135 cm is the distance between the old target and $Q1$).
- 2 The position of the centre of the septum that is given by the intercept of the lines originating from the old (O) the new (O') scattering chamber center (in the case of Fig. 2 making angles $\theta = 6^\circ$ and $\phi = 12.5^\circ$, respectively, with the beam direction)
- 3 The dimension of the gap that accepts all particles scattered in the acceptance cone.
- 4 The value of the integral of the septum magnetic field along the trajectory that is prortional to the bending angle $\beta = \phi - \theta$. ϕ should be, for obvious reasons, the smallest available value. When θ is close to 6° , ϕ is equal to 12.5° . At higher θ values, as will be explained further, θ must be greater than that and requires, as a consequence, very high fields and superconducting coils.

On the other hand, \mathbf{T} , the magnet thickness between the gap and the beam pipe, determines, together with \mathbf{d} , the septum physical length, L . L should be as long as possible because it is proportional to the integral of the magnetic field inside the septum. The longer L , the lower the required field inside the septum and, hence, the current density needed in the septum coils. L cannot exceed, however, the value that makes the septum edge hit the beam pipe (see Fig. 2). For this reason \mathbf{T} should be as small as possible. The limit is give by the thickness of the coils, the dimension of the cryostat and the thickness of the iron between the coils and the beam pipe (it is needed to ensure good mechanical resistance and good magnetic field homogeneity inside the septum).

At θ values close to 12.5° , The limt is reached for ϕ because the septum approaches the $Q1$ edge. High magnetic fields are needed inside the septum. It is useless to decrease the length of the septum in order to allow smaller values of ϕ : the smaller value of the bending angle $\beta = \phi - \theta$ never compensates, from the magnetic field value point of view, the reduced length of the septum. L is therefore, as explained above, fixed by the geometrical layout at $\theta = 6^\circ$ or, in other words, by \mathbf{d} and \mathbf{T} .

Once the septum design parameters are understood, it is not a difficult task playing with the values of \mathbf{d} and \mathbf{T} in order to get a septum design that fits the requirements quoted in Table 2.1. The range of variation of \mathbf{T} , because of the reasons cited above, is not very big. Only reasons of opprotunity, on the other hand, are involved in the choice of \mathbf{d} : a bigger value of this parameters allows a longer septum but decreases the angular acceptance. At last, a value of $\mathbf{d}= 80$ cm was chosen. As a matter of fact, the geometrical acceptance obtained in this case is 4.7 mrad. This value is close to the HRS original design acceptance (7.68 mrad.). Note that the angular acceptance of the new HRS + septum spectrometer, as determined only by \mathbf{d} and \mathbf{T} , that is in absence of the vacuum chamber inside the gap, should be

5.2 mrad. The length of the septum available with this value of \mathbf{d} makes possible, with realistic current densities, the magnetic field integrals needed to bend particles up to 4 GeV/c momentum and scattering angles upto 12.5° . The septum thickness between the gap and the beam pipe (that is \mathbf{T}) changes (it is thicker at the edge closer to Q1) and with a notch in the bottom part of the septum to allow passage of the beam pipe (see Fig 5). This allows a reasonable angular acceptance. The height of the gap was chosen slightly bigger than necessary (25 instead of 20 cm) to provide room for correction coils.

8 APPENDIX B - Optics

To show that the septum is a small perturbation of the HRS spectrometer the following procedure was performed:

- 1 1000 random rays of fixed momentum within the angular and position acceptance were traced by the program RAYTRACE through the spectrometer to the detector plane. The different drift distances to Q1 for rays scattered at very forward angles and at different target points were taken in account.
- 2 By the output of RAYTRACE, for each momentum, the target point coordinates x_0 , θ_0 , y_0 and ϕ_0 were determined as functions of the variables xf , θf , yf , and ϕf on the detector plane.
- 3 For each momentum a new set of rays was randomly generated and traced to the detector plane.
- 4 With the functions described at point 2, the coordinates x_0 , θ_0 , y_0 and ϕ_0 of each of this second set of rays were calculated and then compared to their true values. However, the coordinates xf , θf , yf , and ϕf were not exactly those given by RAYTRACE output, but they were calculated using gaussian laws of probability spread out around xf , θf , yf , and ϕf RAYTRACE output values and with σxf , $\sigma \theta f$, σyf and $\sigma \phi f$ variances chosen in order to simulate the errors on the detector plane coordinates.
- 5 The FWHM of the distributions of the differences between the true and calculated (according to the procedure explained at point 4) values of x_0 , θ_0 , y_0 and ϕ_0 were assumed as the estimate HRS + septum resolutions for these variables.
- 6 For determining the HRS + septum momentum resolution we used the usual first order resolving power formula: momentum resolution $\delta p/p = \frac{\langle x/x \rangle}{\langle x/d \rangle} \delta x_0$ with δ equal to the percentual difference between a ray momentum and the central trajectory momentum but with δx_0 equal to the uncertainty of the x_0 variable AS GIVEN BY THE CALCULATION PERFORMED AT POINT 4 and not by the beam spot size (as usual when a midplane symmetry exists). In this way we tried to estimate the contribution of terms like $\langle x/y \rangle$ to the momentum resolution which is usually forbidden by the midplane symmetry but not zero for the HRS + septum spectrometer. As a matter of fact these terms make the uncertainty on x_0 bigger than in a midplane symmetric environment.
- 7 To compare the results obtained, we repeated the same procedure explained in the points 1-6 for the HRS without septum spectrometer (the version without sextupole and octupole).

Fig. 18 shows the momentum resolution, as well as x_0 , θ_0 , y_0 and ϕ_0 estimated for the HRS + septum spectrometer as compared to the HRS one. The scattering angle of the particles was in both cases equal to 6 degrees (for HRS this is obviously a mathematical game, because it is not able to detect particles scattered at angles smaller than 12.5 degree). The resolutions of the HRS + septum spectrometer system, although always worse than those of HRS, do not differ very much from them.

That shows that the perturbation caused by the presence of the septum to the HRS spectrometer is small.

The result obtained are determined at fixed particle momentum. Nevertheless we think that the DIFFERENCE between HRS with and without septum magnet is a reliable measure of the contribution of the septum magnet to the HRS resolution. To get good momentum resolution, software corrections will be needed. This is also shown by the fact that the polynomials that determine x_0 , θ_0 , y_0 and ϕ_0 as functions of xf , θf , yf , and ϕf change rapidly with the momentum. However, this effect can be reduced by measuring the software corrections at more than six places along the focal plane. A preliminary estimation for the angular and momentum resolution of the HRS spectrometer has been done using the RAYTRACE program with the design data in combination with multiple scattering calculatins to get the contribution from vacuum windows and detector system to simulate the HRS spectrometer with and without septum magnet. The steps performed is essentially the same as in spectrometer tune up: first determine the software corrections using sieve slit and elastic electron scattering from a heavy target and then use the software corrections to analyse data taken with and without sieve slits to judge the angular and momentum resolution. The results are shown in the paragraph 2.3.

9 APPENDIX C - Issues raised by PAC and Expint

9.1 Missing Mass Resolution

The calculations and simulations described above allowed us to evaluate the effect of all the quantities influencing the missing mass resolution. The momentum resolution of the spectrometer has been evaluated taking into account the multiple scattering from the target, target windows (only needed in the case of waterfall target) and the spectrometer exit window. It seems that the multiple scattering from the target and from the target windows give a small contribution (par. 2.3). The dominant term is the spectrometer exit window. A Monte Carlo calculation has been performed to include all the parameters influencing the missing mass resolution, namely the beam energy resolution, the error on the angle, the energy loss in the target. The results are shown in Fig. 3.

9.2 Target

We have seen (par. 2.2) that due to the y_0 acceptance along the perpendicular to the central trajectory, we have 50 cm along the beam line to put the waterfall targets. The number of the foils, the distance among them and the dimension of the cylinder containing the target(s) will be the best compromise between the need to get enough luminosity while keeping a good momentum resolution, and the fact that, being all the foils (but one) not positioned in the object point of the spectrometer, they might illuminate part of the spectrometer where the momentum aberrations can be high. For the targets that are not in the spectrometer median plane, the first drift distance varies causing a “depth of focus” effect.

This fact is not unique to the septum magnet, but common to all the extended targets. This is a potential problem that must be investigated by sieve slit measurements with targets placed in different position along the beam. This problem has been investigated for the Mainz spectrometers (13) where it is shown that the “depth-of-focus” problem can be fixed by using analytical formula. The cell can be made, in principle, big enough for being able to put the windows of the waterfall targets out of the acceptance of the spectrometer. Some shieldig can be put to avoid the increasing of the counting rate from the upstream window to an unacceptable level. This eventual problem obviously arises only for the oxygen target, the others don't have windows.

9.3 Particle Identification

The particle identification will be made by means of the standard HRS detector package with the addition of another aerogel counter. In the electron arm distinction between e^- from π^- and K^- with a rejection ratio $\sim 10^4 - 10^5$ can be achieved using TOF, gas and aerogel Cerenkov counters and shower counters. In the hadron arm, kaons will be separated from pions by aerogel ($n=1.025$ or smaller) and from protons by and) another aerogel with different refractive index (1.06 instead of 1.025) (Fig.

19). In any case, to better understand the PID capability of the detector we have requested (for the (e,e'k) on proton) three days of development time early after the (e,e'p) coincidence capability (with a cryotarget or H₂O) has been established (i.e., winter of 1997). The purpose of the run is to get a kaon spectrum, demonstrating:

- the coincidence capability in the face of large background processes for (e,e'K).
- Kaon PID using the hadron arm aerogel, the TOF between scintillator S1 and S3 in the hadron arm, the TOF through hadron HRS, electron PID, with the electron arm gas cherenkov and shower counter, vertex reconstruction using both spectrometers, missing mass resolution PID, and coincidence timing.

A small aerogel detector with different refractive index will be put on the hadron arm, to allow the separation of kaons from protons and pions. One should note that history and competence of the members of the collaboration in determining PID. As a matter of fact, they have designed, tested and built all the PID part of the HRS spectrometers (Lead glass Calorimeter (Maryland), gas and aerogel cherenkov counters (INFN in collaboration with Saclay and Regina)). Present Hall C experiments using these techniques have been analyzed and performed by this collaboration. Moreover the INFN members have specific experience in kaon identification, having built and tested recently two RICH prototype detectors, one with freon radiator and CsI as photodetector, the other with aerogel radiator and PMT array as photodetector (the first in the world!)(14,15).

9.4 Backgrounds

Possible sources of background in the detector include neutrons, multiply scattered electrons and hadrons, and “junk” created by photons and electrons from the target which interact with the pole faces of the magnet and produce a spray which is directed toward the detectors. This problem has been addressed for the parity experiment. Calculations have been performed, by Z.E. Meziani (16) for the He-4 target, for 12.5 degrees, considering three sources emitting photons: direct bremsstrahlung, forward bremsstrahlung followed by Compton scattering and the radiative Moller scattering. The conclusion was that the rate over a full detector area is not critically high and should not be a serious concern because of the large bend angle of the HRS dipole.

Similar calculations for our case are underway. We estimate that the flux should be equivalent. In fact the increasing relative flux due to the lower angle should be compensated by the thinner target. Moreover we have calculated the solid angle for trajectories entering the dipole. The solid angle is practically zero for particles of low energy (Fig. 20). The simplest way to control these sources of background are through shielding and baffling. The Hall A shielding is still being constructed and should be adequate. Baffling is being done for this experiment actively through the use of the magnetic fields. Low energy particles are swept away by first the septum (horizontally), next the quadrupoles (both horizontally and vertically) and then the dipole (vertically). The septum setup will therefore have reduced backgrounds compared to the normal running situation in Hall A.

9.5 Septum Magnets heating due to beam radiation

Calculations have been done to estimate the amount of radiation that the septum are expected to see, the radiation backgrounds that can be produced by the beam,

and the amount of radiation the experiment will produce. The estimations come from the computer code “elec3” written by Geoffrey Stapleton to model anticipated radiation levels for TJNAF experiments. The calculation has checked the “radiative losses”. The number from the code is 0.312 W, in agreement with Dubna calculation. So we think that beam heating is not a significant source of heat in the magnet. We will have more information from the dose measurements that are been doing in the commissioning period.

9.6 Radiation Hardness

Assuming that the septum magnets will operate for about 4 long experiments (i.e. one year of high current beam, equivalent to our running) we will be able to estimate how much radiation the magnets should receive during their lifetime.

9.7 Magnet Activation

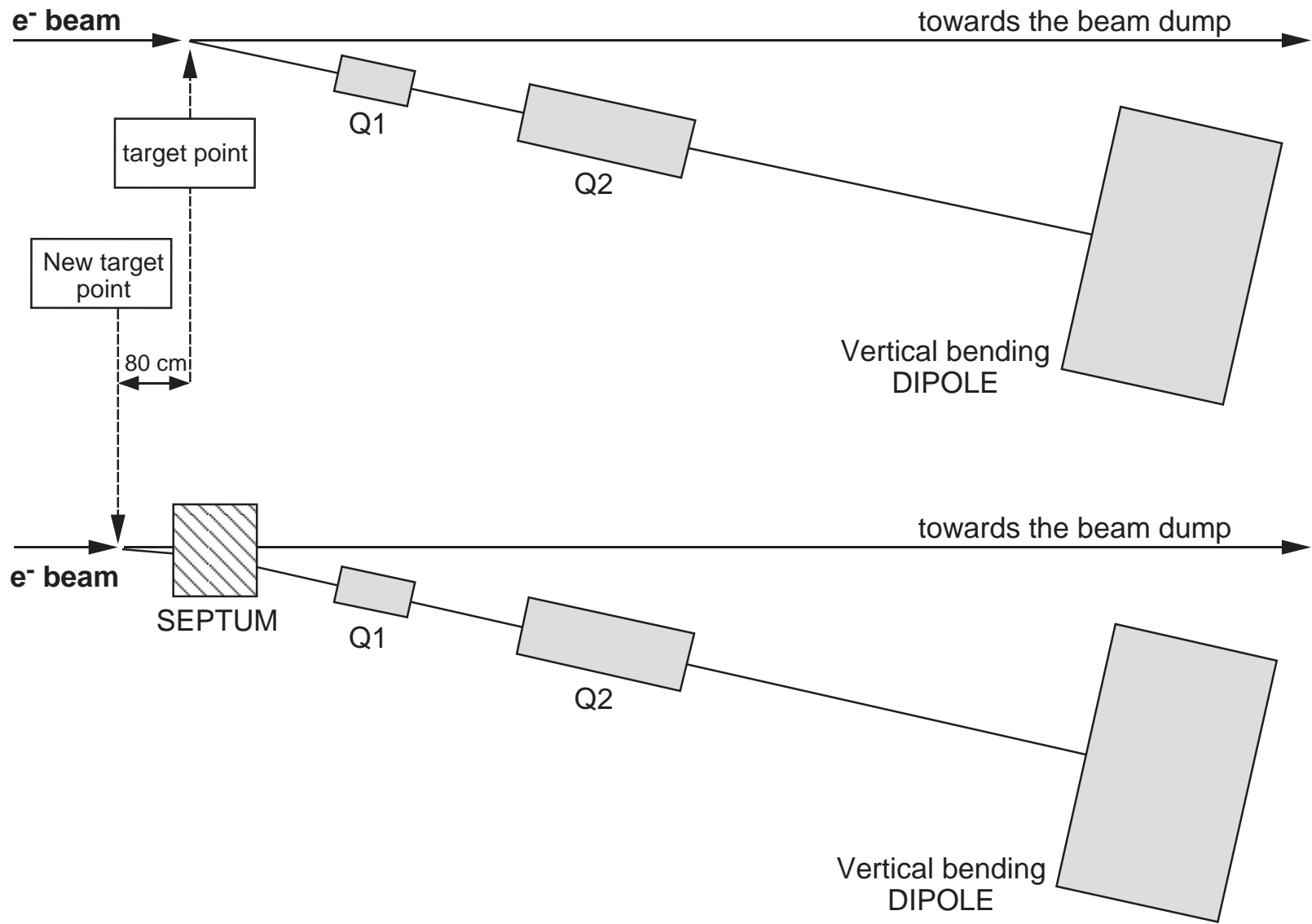
The septum magnets will, at some level, become activated by the beam. Jefferson Lab has procedures in place to handle equipment which has become activated. The exact procedures followed will depend on the measured level of activation, however the amount of beam which the magnets will be exposed to is limited by the short duration of the experiment and the thin targets used (although beam currents are reasonably high).

The procedures and the techniques were put in place for accelerator magnets; in principle this is not different. The amount of time required for removal will utilize an (unknown) amount of time for the magnets to “cool down”, although obviously one to two days will also be required to warm up the cryogenic parts before disconnecting the magnet.

10 REFERENCES

- 1) PR-94-107, Hall A Proposal " 1 p Shell Hypernuclear Spectroscopy " S. Frullani, F. Garibaldi, P. Markowitz, T. Saito
- 2) LOI-94-103, Hall A, " High resolution Electroproduction of Light Hypernuclei" T. Saito
- 3) PR-94-108, Hall A Proposal " Electroproduction of Kaons up to $Q^2 = 3$ (GeV/c)² O.K. Baker, G.C. Chang, S. Frullani, M. Iodice and P. Markowitz
- 4) P. Markowitz, G.C. Chang, E. Cisbani, S. Frullani, F. Garibaldi, M. Iodice, G.M. Urciuoli, J. Leroise, S. Nanda, " Forward angle physics in Hall A" CEBAF Tech Notes TN 94-034 (05-09-94)
- 5) CDR - CEBAF BASIC EXPERIMENTAL EQUIPMENT - April 13, 1990 (revised)
- 6) J. Alcorn, J. LeRose, S. Nanda, E. Offermann, "The Hall A Sextupole Crisis - An Evaluation of the Magnitude of the problem and Possible solutions (2/16/95)
- 7) G.T. Danby, J.W. Jackson and S.T. Lin, "High Field Iron Magnets" Brookhaven National Laboratory, Upton, New York, IEE Transaction on Nuclear Science Vol. 1971
- 8) J. Allinger, G. Danby, J. Jackson, A. Prodell " Ultra stable High Field Superconducting Dipoles" IEE Transaction on Nuclear Science Vol. NS-24, n. 3, June 1977
- 9) T. W. Donnelly and S.R. Cotanch, "Using Kaon electromagnetic production to study Hypernuclear Systems
- 10) A. M. Baldin and A.D. Kovalenko, " The status of the Dubna relativistic heavy ion facility", CERN bulletin, 14/93, 4, 1993
- 11) A. M. Baldin, S. A. Averichev, Yu D. Beznogikh, A.M. Donyagin, E.I. D'yakchov et al, "Nuclotron status report", IEE Trans. on Nucl. Sci., Vol. 3, N4, pp 3247-3249, August 1983
- 12) Cryogenic System of the Nuclotron - A new Superconducting Synchrotron. E9-93-273 - JINRS - Dubna - Russia, Submitted to the Cryogenic Engineering Conference, 12-16 July, Albuquerque, USA
- 13) Mafred Korn. Diploma Thesis. Mainz
- 14) Status Report RD26 - CERN/LHCC 96-20 LDBR - 21 feb. '96
- 15) R. Forty, "Ring Imaging Cherenkov Detectors for LHC-B", Beauty96. Rome - June '96
- 16) Z.E. Meziani. CEBAF TN. 92-039. Photon flux Computation for the HRS septrometers at Forward Angles"
- 17) T. Hasegawa et al.: Core excited states of ¹²C lambda hypernuclei formed in the (pi+,k+) reaction, INS-Rep-1037, University of Tokyo, 1994

Figure 1: Schematic Layout of the proposed modifications to the HRS setup



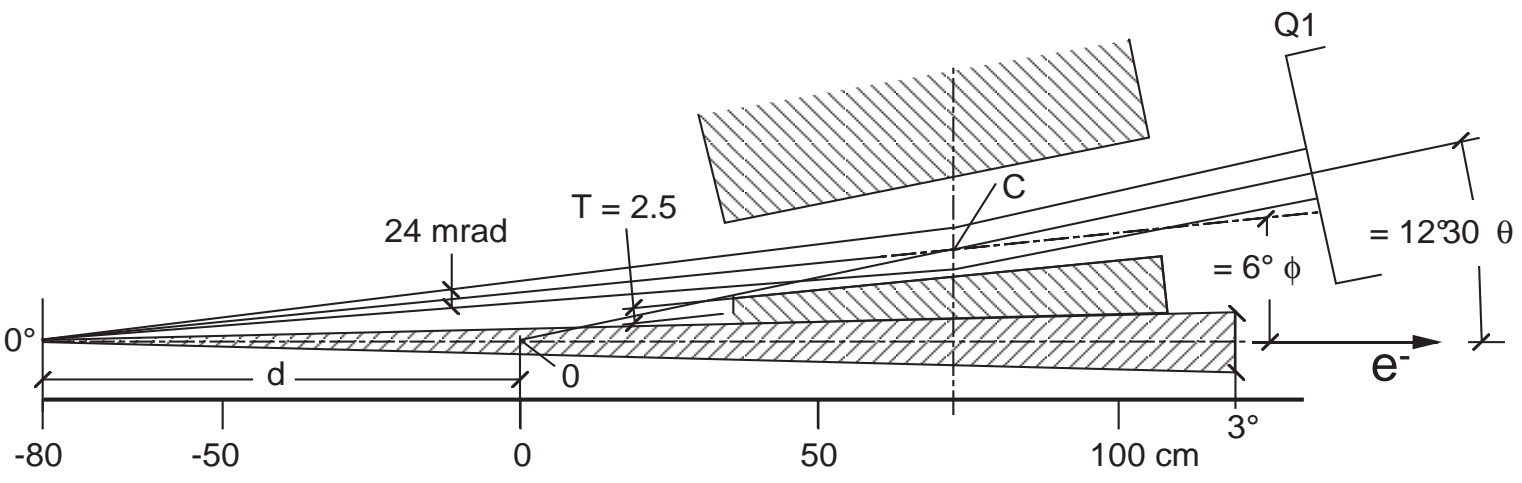


Figure 2: Layout of the septum insertion

MC simulation for E_missing resolution

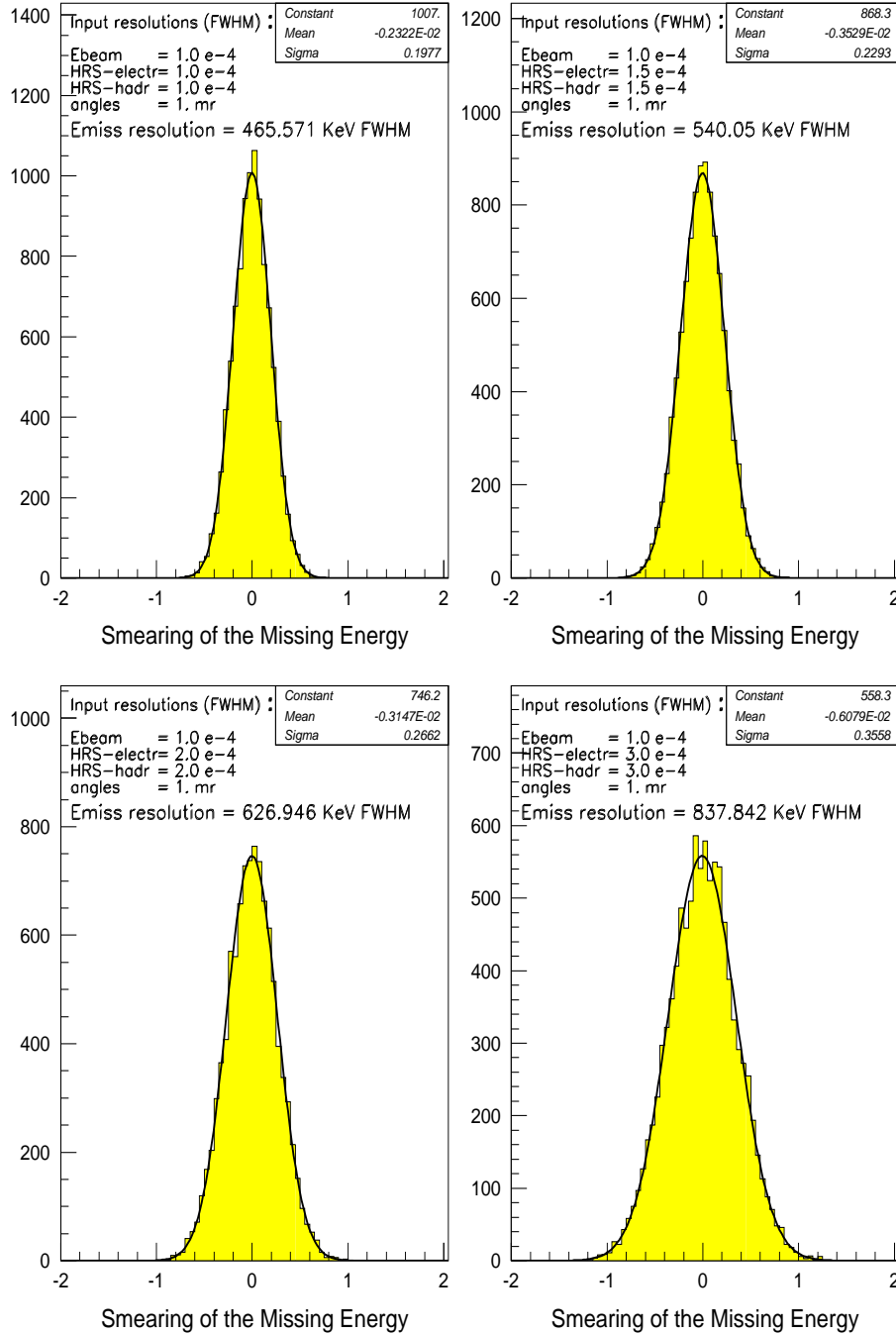


Figure 3: Expected Missing Mass Resolution as function of various beam and momentum resolution

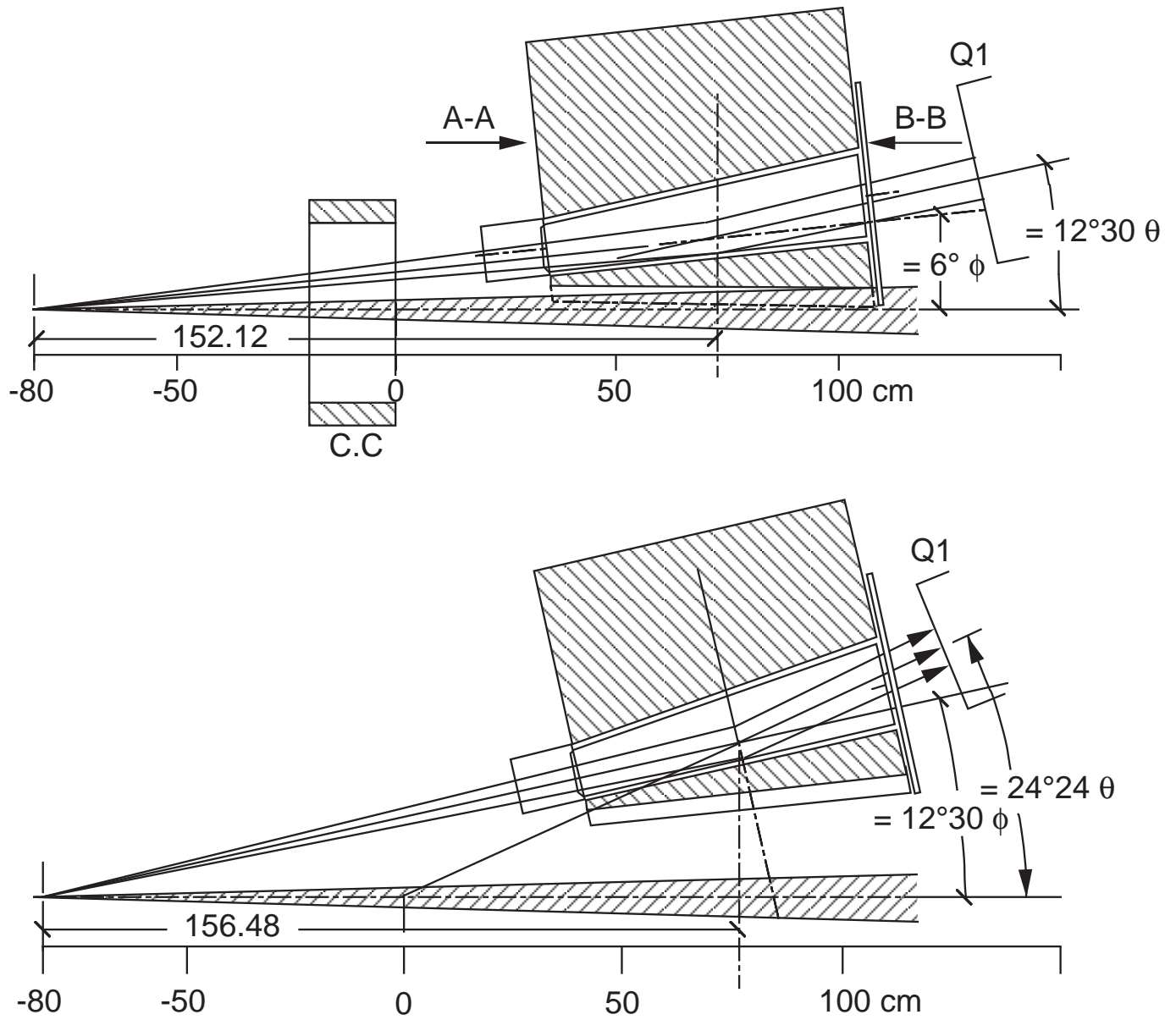


Figure 4: Layout of the system in the “extreme” angular conditions. The septum is shown at 70 cm and the corrector coils (CC) are shown at -10 cm. All angles are in degrees and minutes.

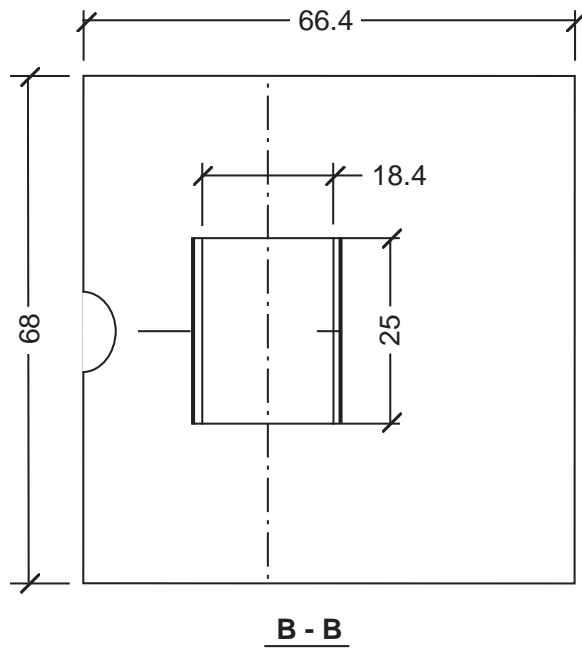
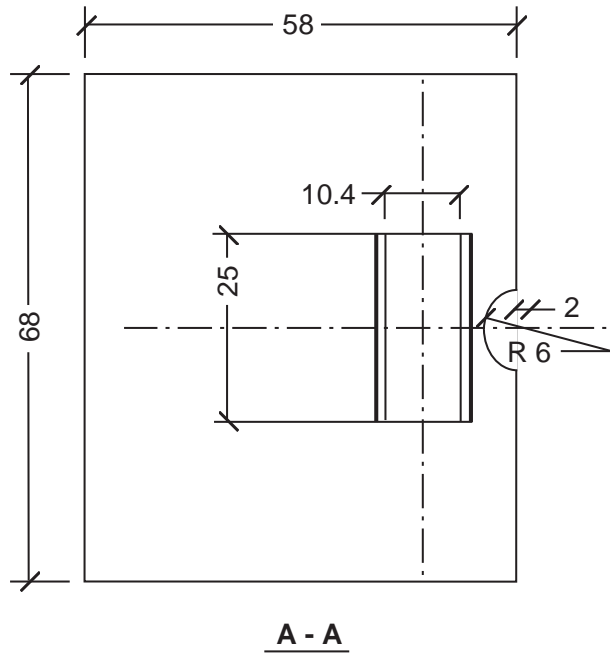


Figure 5: Layout of the system in the “extreme” angular conditions.

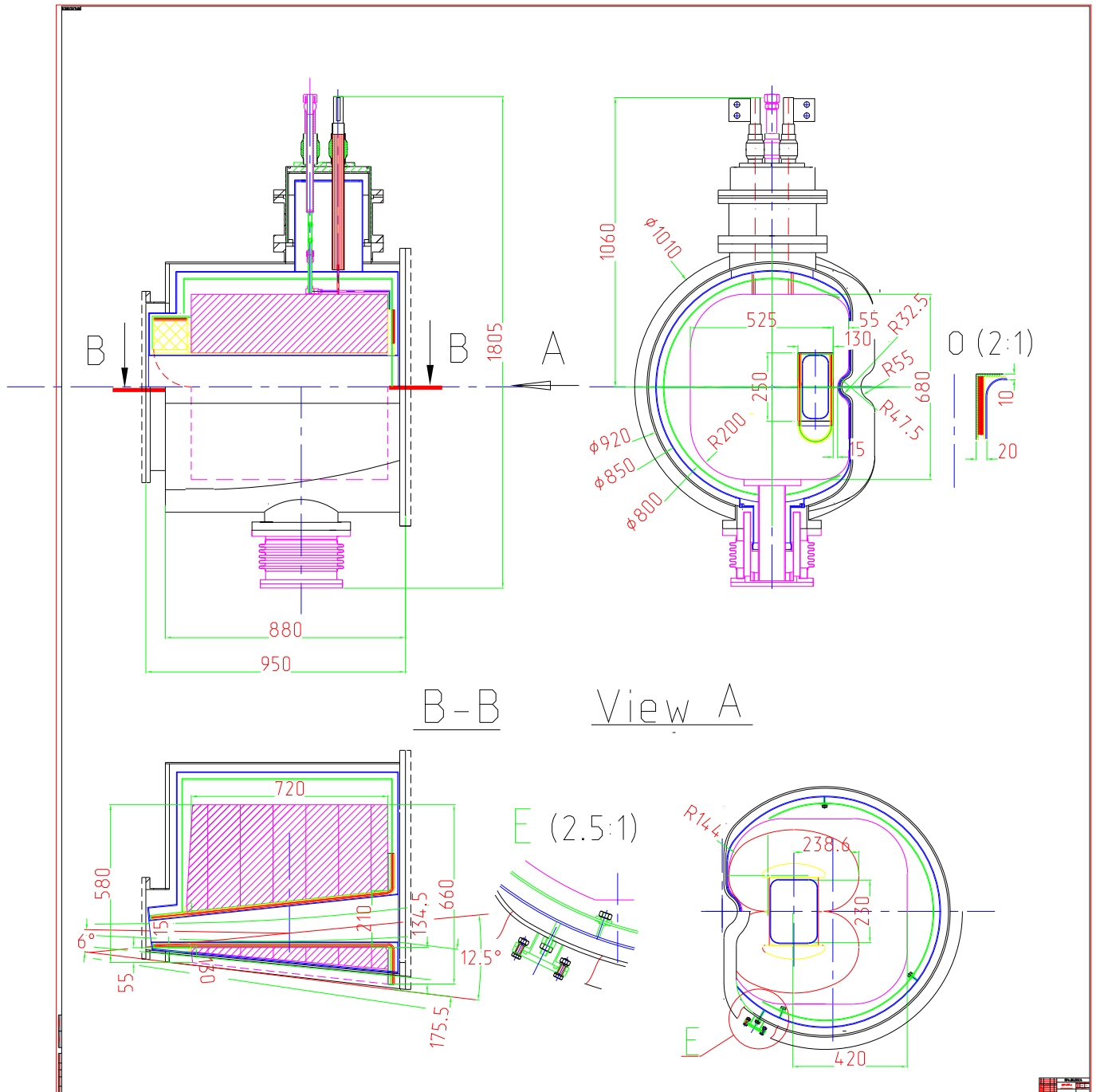


Figure 6: General view of the septum magnet unit inside the cryostat.

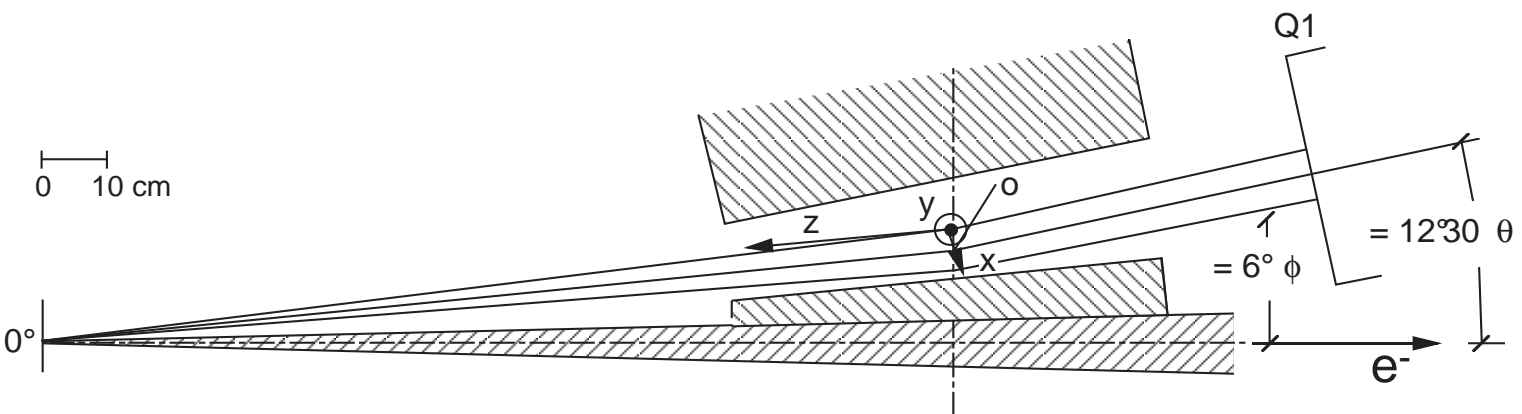


Figure 7: Septum layout with the reference frame used for the field calculation.

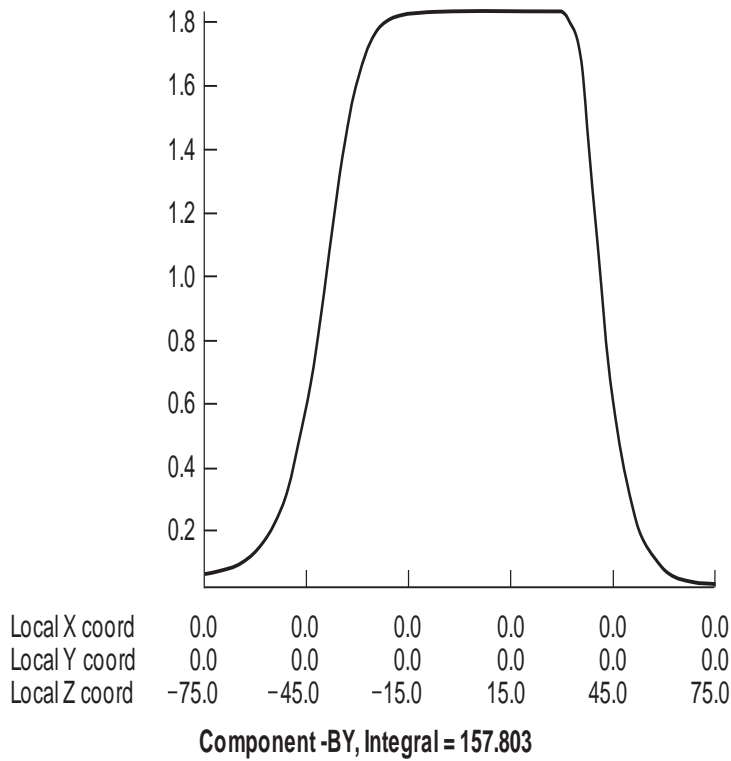


Figure 8: Magnetic field behaviour along the longitudinal (z) coordinate of the septum midplane ($y=0$) at the centrum of the septum ($x=0$) and $\phi = 6^\circ$.

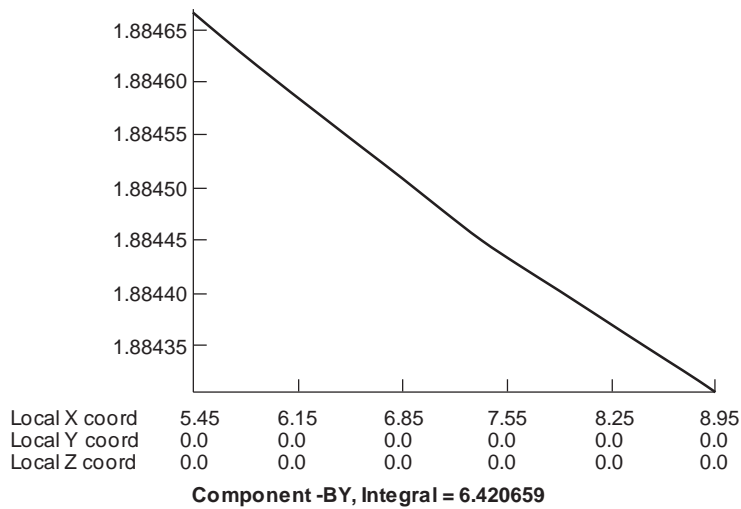


Figure 9: Magnetic field along the transverse coordinate ($z=\text{constant}$) at the center and $\phi = 6^\circ$.

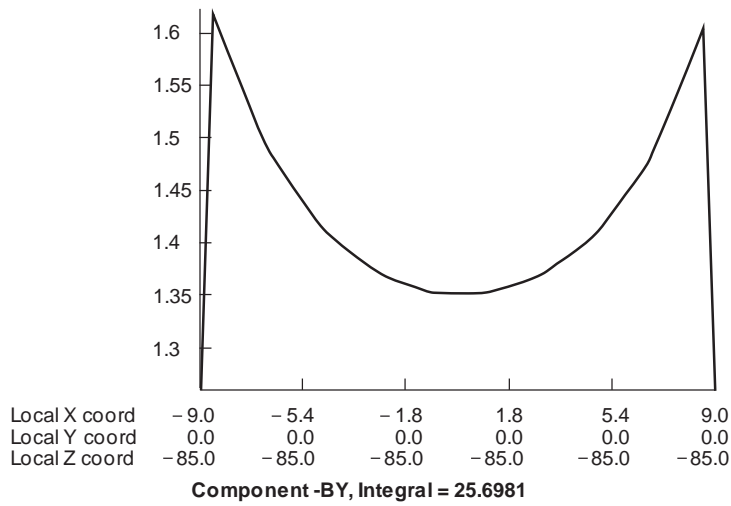


Figure 10: Magnetic field along the transverse coordinate ($z=\text{constant}$) at the exit position and $\phi = 6^\circ$.

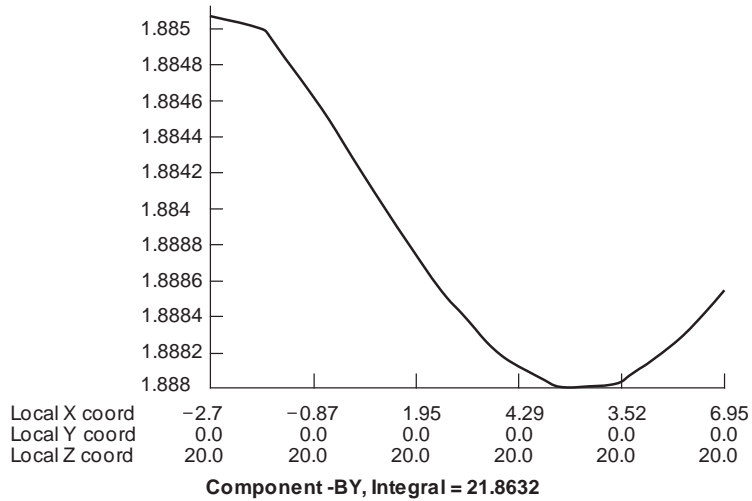


Figure 11: Magnetic field along the transverse coordinate ($z=\text{constant}$) at the intermediate and $\phi = 6^\circ$.

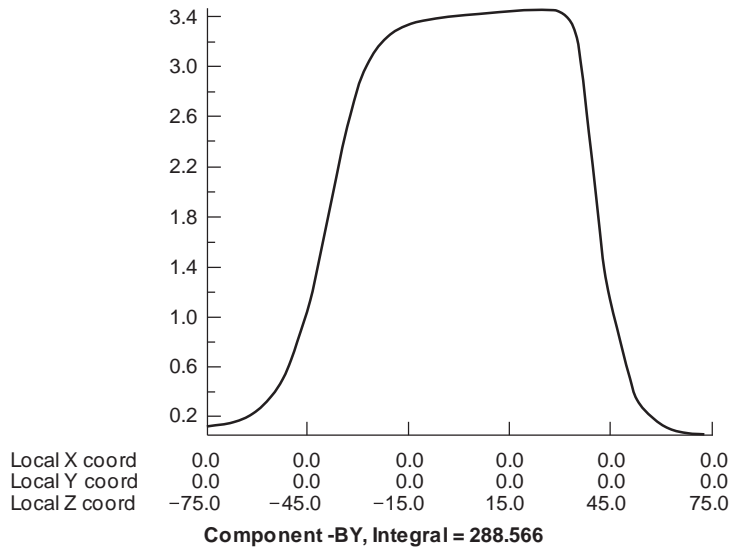


Figure 12: Magnetic field along the longitudinal coordinate ($z=\text{constant}$) at the center ($\phi = 12.5$ degrees)

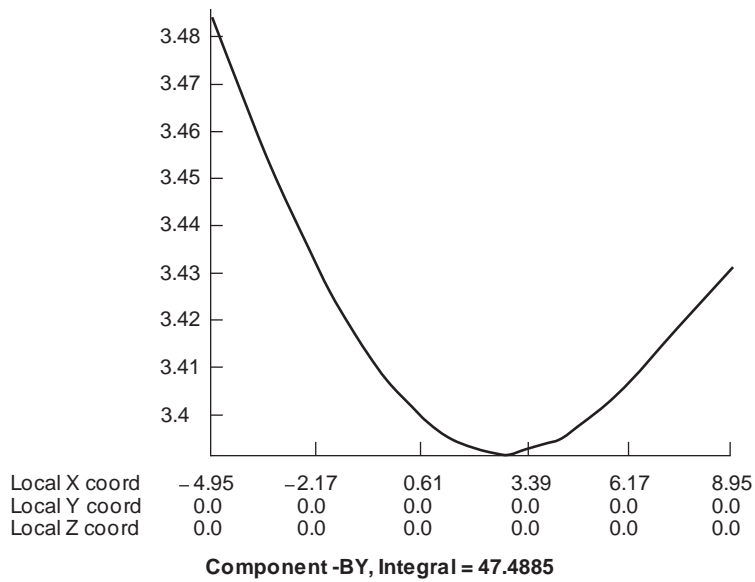


Figure 13: Magnetic field along the transverse coordinate ($z=\text{constant}$) at the center position ($\phi = 12.5$ degrees)

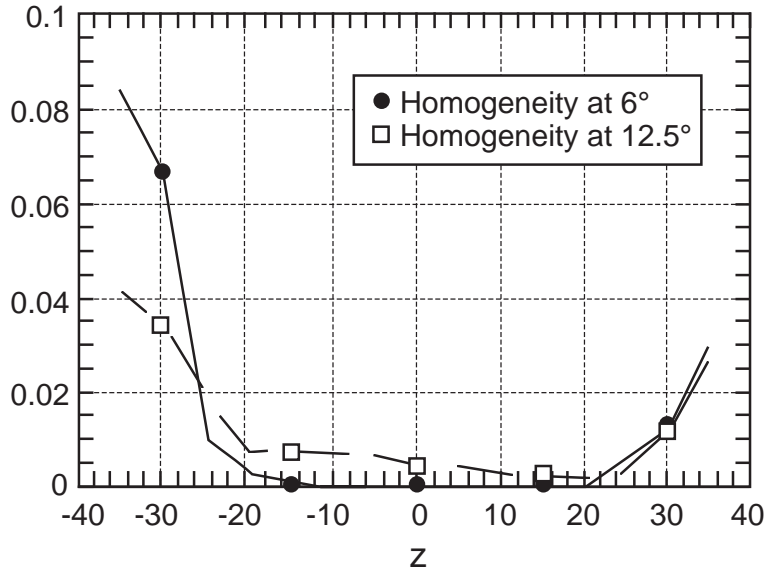


Figure 14: Field Homogeneity in the region crossed by the particles as a function of the longitudinal coordinate of the septum (for 6 and 12.5 degrees)

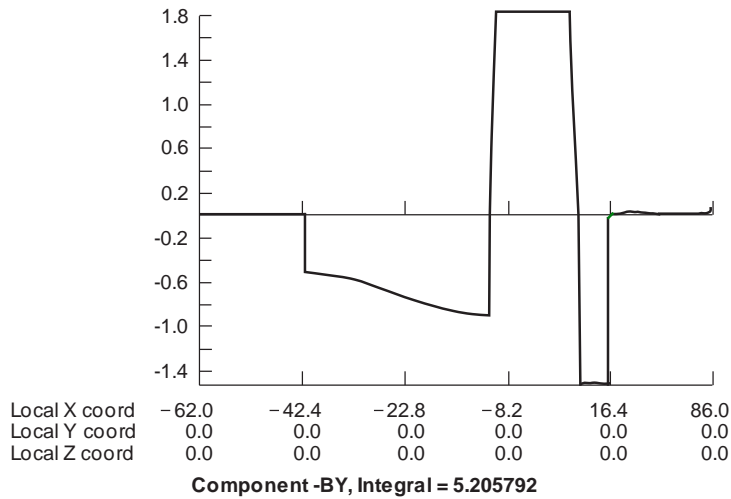


Figure 15: Magnetic induction at the center of the septum gap ($-5.2 < x < 9.2$) and in the iron.

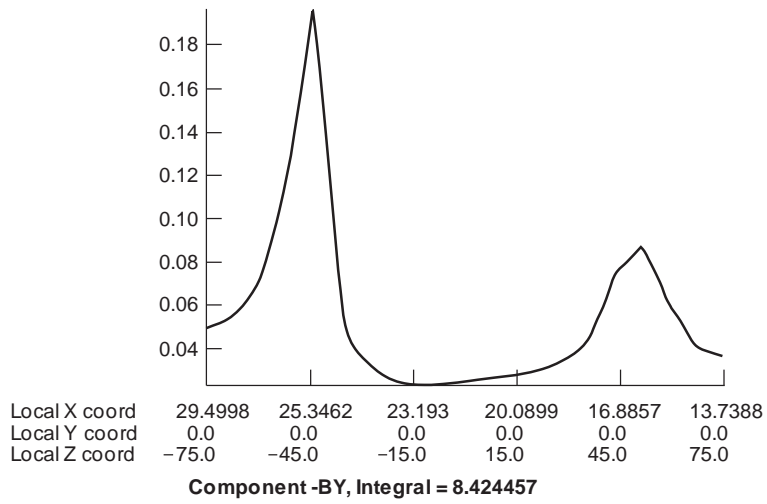


Figure 16: Stray field generate4d on the beam pipe in the case 6 degrees

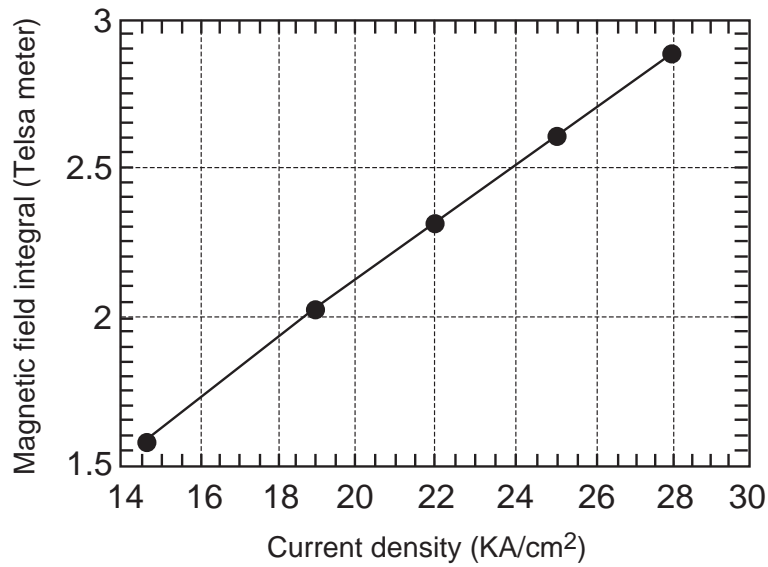


Figure 17: Magnetic field integral as function of the current density

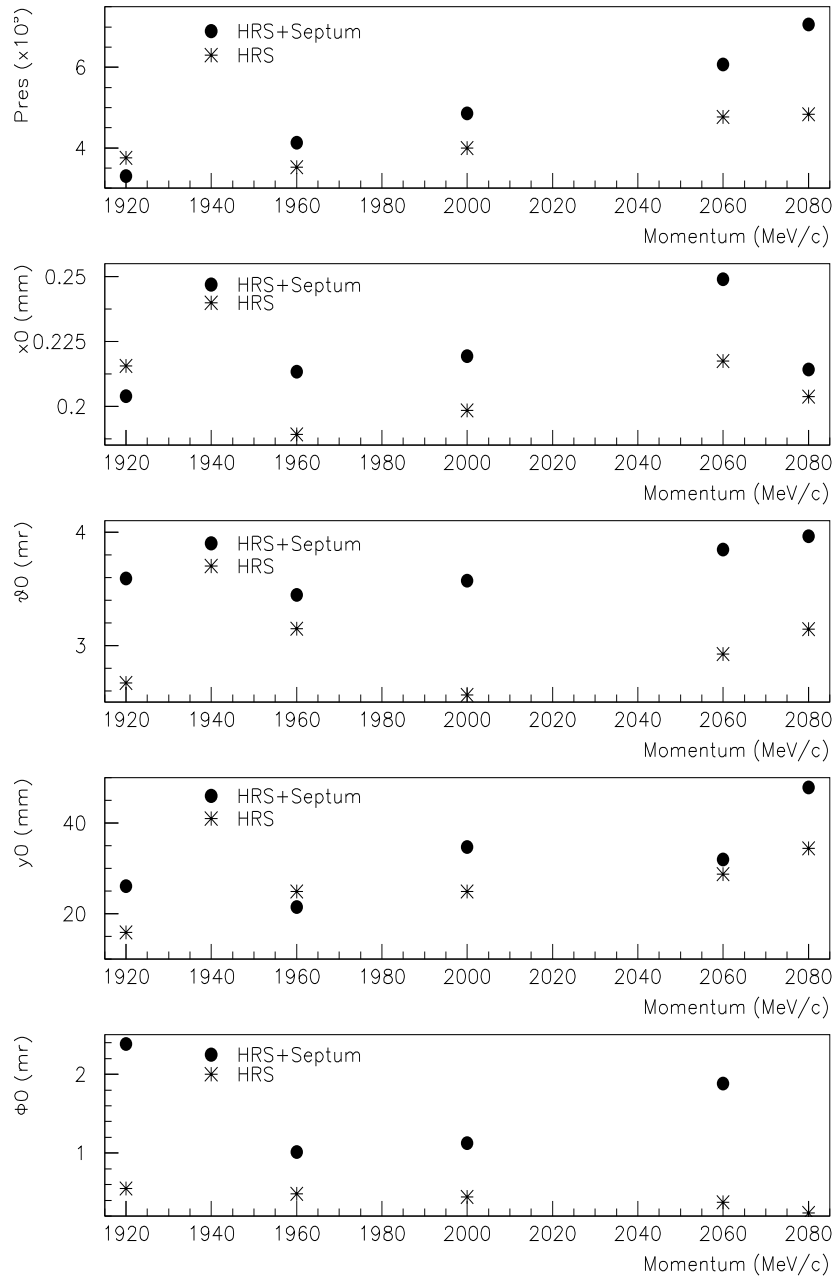


Figure 18: Comparison between HRS and HRS + Septum. All resolutions are FWHM.

Particle Identification using aerogel Cherenkov

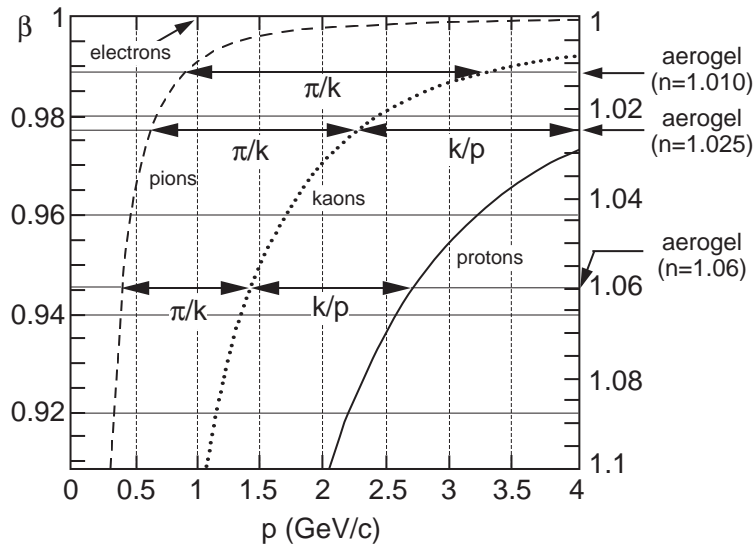


Figure 19: PID by threshold aerogel

Solid angle as function of momentum

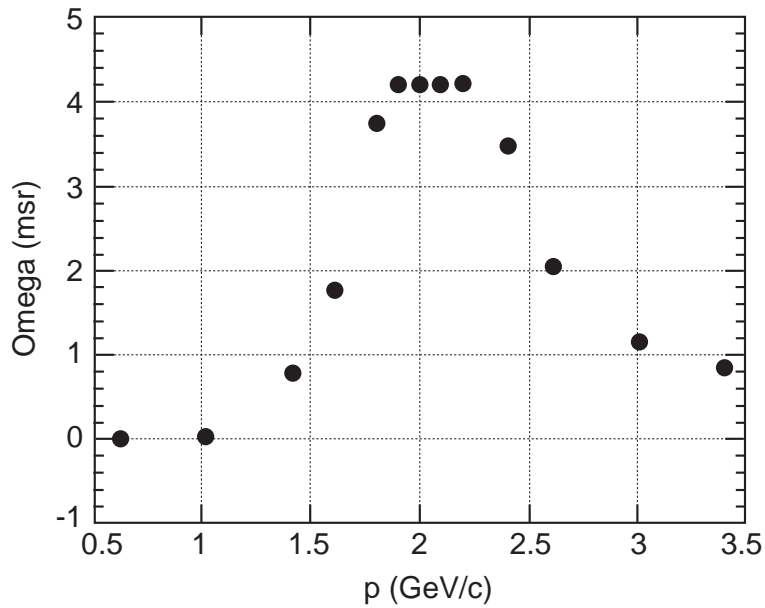


Figure 20: Solid angle for trajectories entering the dipole